Contamination effects on the lift force of ellipsoidal air bubbles rising in saline water solutions

Hessenkemper, H.; Ziegenhein, T.; Lucas, D.;

Originally published:

April 2019

Chemical Engineering Journal 386(2020), 121589

DOI: https://doi.org/10.1016/j.cej.2019.04.169

Perma-Link to Publication Repository of HZDR:

https://www.hzdr.de/publications/Publ-28493

Contamination effects on the lift force of ellipsoidal air bubbles rising in saline water solutions

H. Hessenkemper[1], T. Ziegenhein[1,2], D. Lucas[1]

[1]Helmholtz-Zentrum Dresden-Rossendorf e.V., 01314 Dresden, Germany

[2]School for Engineering of Matter, Transport and Energy, Arizona State University, Tempe, AZ 85287, USA

* Corresponding author. Tel.: +49 3512602620; fax: +49 3512603440.

E-mail address: h.hessenkemper@hzdr.de (Hendrik Hessenkemper)

Abstract

The lift force is known to strongly influence the lateral bubble distribution in bubbly flows and is therefore an important force that has to be modeled in corresponding CFD simulations. For ellipsoidal bubbles, which are mostly present in industrial cases, the strength as well as the direction in which the lift force acts is determined by the bubble deformation. The bubble deformation however, can strongly be reduced when surface-active contaminations like salts are present in the liquid bulk, which implies a change of the lift force by contaminations too. In the present work, lift coefficients for single bubbles rising in aqueous NaCl solutions were determined to investigate the influence of such an inorganic surfactant on the lift force. For this purpose, a recently developed method by Ziegenhein et al. [*Int. J. Multiphase Flow*, Vol. 108, 11-24 (2018)] is used, which is capable to measure the lift force in low viscous liquids. Besides the lift force, the bubble shape and slip velocity were studied in detail to connect the results to known contamination effects, which showed different behavior in dependence on the salt concentration. The results

reveal that the contamination level plays an important role on changes of the lift force in comparison to clean bubbles. Up to a concentration of 1.0 mol/l the salt has only a weak effect on the lift force of larger bubbles. The lift coefficients of smaller bubbles however, clearly show significant changes, which were also reflected in a change of the bubble shape. However, some findings could only be connected to the slip velocity, which implies a connection of the lift force to more than just the shape.

Keywords. Lift coefficient; Bubbly flows; Contaminations; Bubble shape; Slip velocity; Sodium chloride

1. Introduction

Bubbly flows consist of gas bubbles dispersed in a continuous liquid phase and occur in several industrial fields like chemical reactors or nuclear power plants. A deep knowledge of the ongoing phase-interactions in these kind of flows is of great importance to increase the performance and higher safety standards in the corresponding application. One important non-drag interaction is the lateral lift force, which acts on bubbles rising through a liquid shear field. The lift force has a major influence on the lateral void distribution and depending on its sign, it can stabilize or destabilize a flow regime (Lucas, et al., 2005). Reliable models of the lift force are crucial to simulate such kind of flows with multiphase CFD tools. However, many existing investigations were performed in purified systems, although already small amounts of surface-active contaminations are well known to strongly change the behavior of a single bubble like its slip velocity or its coalescence ability (Clift, et al., 1978). Literature concerning contamination effects on the lift force are very limited and existing studies were not able to determine lift coefficients over a wide range of bubble sizes so that only for a limited number of cases and used additives data exist (Takagi & Matsumoto, 2011). Especially the influence of ionic surfactants like salts has not been investigated so far, although numerous studies are available addressing the coalescence inhibition due to the presence of salt (an overview can be found in Firouzi, et al., 2015). For a better understanding and accurate simulations of relevant applications containing bubbly flows and salts (e.g. flotation cells or waste water treatment plants), possible effects on the lift force have to be evaluated, which is the main subject of the present work.

For small, spherical bubbles passing a linear shear field the lift force acts in the direction of decreasing liquid velocity, which is in the direction of the wall in a classical upward pipe flow (Legendre & Magnaudet, 1997). From the definition of the lift force (Žun, 1980), this

is accounted for with a positive lift coefficient C_L. With increasing size and therefore more pronounced deformation, it was found that bubbles tend to move in the direction of increasing liquid velocity and form a core-peak void distribution profile in upward pipe flows or bubble columns. The corresponding C_L value changes from a positive value to a negative value for this kind of bubbles, which has been proven by several investigations (Kariyasaki, 1987) (Ervin & Tryggvason, 1997) (Bothe, et al., 2006) (Dijkhuizen, et al., 2010) (Lucas & Tomiyama, 2011) (Aoyama, et al., 2017). Through the analysis of numerical experiments Tomiyama et al. 1995 stated that the interaction of a slanted wake behind a deformed bubble and the governing liquid shear field leads to this change of the lift force direction. Later, Tomiyama et al. 2002b determined lift coefficients for single bubbles of different size in higher viscous liquids and developed a widely used correlation for C_L, which is based on the major axis of a bubble. Adoua et al. 2009 conducted numerical simulations with fixed, oblate spheroidal bubbles and related the C_L sign change to the vorticity generation at the bubble surface, which is again dependent on the bubble deformation and the mobility of the bubble surface (Fan & Tsuchiya, 1990).

The bubble deformation as well as the surface mobility are both reduced when surfactants are present in the liquid bulk. Responsible for this is a Marangoni-stress at the bubble surface resulting from a surface tension gradient. This surface tension gradient again is caused by an unequal distribution of absorbed surfactant molecules on the surface, since these molecules are shifted to the rear of the bubble due to the rising bubble motion (Cuenot, et al., 1997) (Hosokawa, et al., 2017). As a result of this Marangoni-stress the deformation is reduced (Aoyama, et al., 2018) and the surface is immobilized, which increases the drag of the bubble and lowers its slip velocity (Tomiyama, et al., 2002a) (Krzan, et al., 2004).

Although the mentioned changes of the surface behavior also imply an effect on the lift force, available work regarding this topic are rather limited in the literature. Tagaki et al. 2008 conducted experiments in a bubble column and observed strong bubble migration to the wall region when tap water without any added substance was used. These clusters vanished when organic surfactants were added to the flow. For a more detailed analysis of the ongoing changes they conducted experiments with single bubbles in a laminar Poiseuille flow. With different contamination levels of added 3-Pentanol and Triton X-100 they revealed that C_L for 1 mm bubbles decreases from 0.5 with only minor contaminations to 0 for fully contaminated bubbles, which is in agreement with the numerical results from Fukuta et al. 2008 for 1-Pentanol. Additionally, they tried to determine C_L with a turbulent background flow but were not able to overcome the irregular changes of the bubble rising path (Takagi, et al., 2009) (Takagi & Matsumoto, 2011). Lu et al. 2017 simulated a turbulent bubbly flow with and without contaminated bubble surfaces and confirmed the suppression of bubble clusters at the wall with contaminated smaller bubbles. For larger bubbles, they observed a reduced contamination effect on the void distribution. Recently, Hayashi & Tomiyama 2018 investigated contamination effects on the lift force with numerical simulations of single bubbles rising in higher viscous liquids. The results also reveal a decrease of C_L when contaminations are present. As another interesting aspect the authors showed, that in the case of a homogenous surface tension reduction and therefore no significant Marangoni force, still a reduction of C_L could be observed.

To the authors knowledge this is the first work addressing the contamination effect of an inorganic surfactant on the lateral lift force of single bubbles in dependence of size and deformation. Three different NaCl concentrations were investigated, whereby during the analyses special attention was drawn to the bubble shape and the slip velocity as

indicators for ongoing surface contaminations. With the used experimental configuration this work aims to provide a better understanding of the lift force behavior under industrial relevant conditions.

2. Experimental description

2.1. Experimental method

To determine the lift force acting on bubbles a shear field is required in the liquid flow. Often a rotating belt is used in the literature to generate a linear velocity gradient like for example in the work of Tomiyama et al. 2002b or Aoyama et al. 2017. This technique works well in high viscous liquids but does not provide a strong enough shear field in low viscous liquids like water. In the present work, a new method introduced by Ziegenhein et al. 2018b is used, which is briefly described in the following. A detailed description and discussion of this method can be found in the mentioned publication.

The basic idea is to use a volume force instead of a wall force to generate a strong enough shear field. Caused by the injection of an additional bubbly flow at the side of a bubble column, an elongated vortex is induced in the rest of the column as indicated on the left side in Figure 1. The vertical velocity component of the vortex has a linear gradient and therefore a linear shear field at the region used for the measurements. Single bubbles are then continuously injected at the opposite and rise through this shear field, where the bubbles are recorded with high-speed cameras and analyzed with post-processing routines.

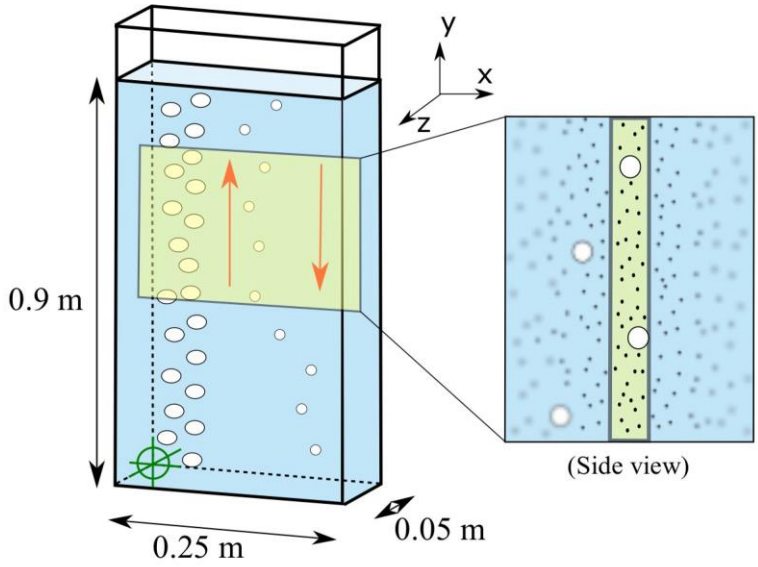

Figure 1: Experimental setup (left) with the thin sharpness field (right). The red arrows show the liquid flow direction inside the column caused by the driving bubbles at the side.

Besides the generation of a linear shear field in low viscous systems, the work of Ziegenhein et al. 2018b provides a suitable averaging procedure to address the bubble movement at high Reynolds numbers (e.g. bubble rise path oscillations) and slightly turbulent background flows. In a first step of the averaging procedure, the measured bubbles are transferred to a rectilinear grid with a cell size of 0.5 mm, which is then used to calculate the void distribution for the field of view. Afterwards, an average bubble rise path is determined using the void maxima along the height. Together with the average liquid velocity field, the lift force can be calculated along this rise path with the following force balance:

$$\overline{\vec{F}}_{Lift} = \overline{\vec{F}}_{Buoyancy} + \overline{\vec{F}}_{Drag} + \overline{\vec{F}}_{VirtulMass} \tag{3}$$

The substitution with the corresponding force terms yields:

$$\overline{C}_L \rho_G \left(\overline{\vec{u}}_G - \overline{\vec{u}}_L\right) \times rot\left(\overline{\vec{u}}_L\right) = \Delta\rho\vec{g} + \frac{3}{4}\frac{1}{d_B} C_D \rho_L \left|\overline{\vec{u}}_G - \overline{\vec{u}}_L\right| \left(\overline{\vec{u}}_G - \overline{\vec{u}}_L\right) + C_{VM}\rho_L \frac{D\overline{\vec{u}}_L}{Dt} \tag{4}$$

The virtual mass coefficient C_{VM} is calculated as proposed by Tomiyama 2004, which is close to 0.5. The drag coefficient C_D is calculated via a vertical force balance with the assumption that the vertical lift force is negligible.

2.2. Setup and materials

The experimental facility is the same as the one used in Ziegenhein et al. 2018b and consists of a rectangular bubble column made of Plexiglas. Figure 1 shows a sketch of the column with the corresponding dimensions. At the beginning of each measurement the column was filled with deionized water together with NaCl (99.9% purity) to a fill height of 900 mm. The driving bubbles generating the shear field were injected through four 0.6 mm spargers with a constant flowrate of 0.8 l/min. The single bubbles were generated with flowrates up to 15 ml/min and various sparger sizes, providing single bubbles in a size range of 2.2 – 6.5 mm. Smaller bubbles up to a size of about 4.5 mm were generated with sparger sizes of 0.12 – 2.0 mm inner diameter. To generate larger bubbles, small plastic tubes were put over the sparger outlet, which increased the effective sparger diameter. The whole setup was background illuminated with a 200 W LED lamp. A diffusor plate was installed between the light source and the column to ensure a homogenous illumination of the test section. All measurements were conducted under ambient pressure and room temperature between 20 – 22 °C.

To determine the required parameters the flow was recorded with an IDS UI-3160CP camera and a 135 mm f2.0 Walimex Pro foto lens. The images were recorded with a framerate of 180 fps and a resolution of 1920x1200 pixels, resulting in a pixel size of 53 µm. For calculating liquid and gas bubble velocities, pairs of double images were recorded with a delay of 75 ms between two image pairs, which were continuously streamed to a PC. To analyze a sufficient amount of single bubbles and overcome the mentioned challenges in low-viscous flows, a measurement time of 90 mins was chosen. This results

in approximately 60.000 image pairs and therefore 60.000 liquid velocity fields as well as 50.000-140.000 single bubbles after processing the images for every single experiment. Through the long measurement time and high data amount, a large number of repetition measurements was not realizable. Nevertheless, at least two experiments were conducted per bubble size and concentration to test the reproducibility of the obtained results.

The first used concentration of 0.2 mol/l NaCl is well known to inhibit coalescence nearly complete, which already indicates a contamination of the bubble surface (Firouzi, et al., 2015). In parallel to the present work, Ziegenhein et al. 2018a analyzed the shape of bubbles rising in different bubble column configurations and could not identify a clear contamination effect on the bubble deformation up to a concentration of 1.0 mol/l. In contrast to this, Quinn et al. 2014 revealed a quite strong contamination effect on the shape as well as on the slip velocity already for a lower NaCl concentration of 0.4 mol/l. Therefore, the second investigated concentration was 0.4 mol/l to elaborate the existing discrepancy from the mentioned sources. The highest used salt concentration in this work was 1.0 mol/l, since for higher salt concentrations a blocking of the spargers during the long measurement time could be observed. A possible explanation for this could be crystallization processes at the sparger tip, which were also reported by Orvalho et al. 2009. All spargers as well as the column were thoroughly cleaned with deionized water in between two experiments to ensure that no salt remained in the setup and therefore to prevent such blocking effects.

The values for viscosity and density for the different solutions were taken from data by Liu et al. 2009. For calculating the corresponding surface tension, the following fit from Nayar et al. 2015 was used:

$$\sigma = \sigma_W(1 + 3.766 \cdot 10^{-4} \cdot S + 2.347 \cdot 10^{-6} \cdot S \cdot T) \quad (1)$$

where S is the salinity in g per kg, T the temperature in Kelvin and σ_W the surface tension of pure water. These values were used to assess the development of C_L with the following dimensionless numbers:

$$Eo = \frac{\Delta\rho g d_B^2}{\sigma}, Eo_\perp = \frac{\Delta\rho g d_{Major}^2}{\sigma}, Re_\perp = \frac{\rho v_{rel} d_{Major}}{\mu}, E = \frac{d_{Minor}}{d_{Major}}. \quad (2)$$

The modified Eötvös number $Eo_\perp$ and Reynolds number $Re_\perp$ are calculated with the major axis d_{Major} of the bubble, while the conventional Eötvös number Eo is calculated with the diameter of a volume equivalent sphere d_B. The aspect ratio E is the ratio of the bubble minor axis d_{Minor} to the bubble major axis d_{Major}.

2.3. Measurement techniques

In the original work by Ziegenhein et al. 2018b the liquid velocities were measured with conventional PIV using a laser-sheet to illuminate the tracer particles. The single bubbles were separately recorded with stereoscopic shadowgraphy. Afterwards the results of both measurements were combined to calculate the corresponding lift force. Through the use of a small depth of field (DOF) and a background illumination, bubble properties as well as liquid velocity fields can be measured simultaneously in a quasi-2D sharpness region (Bröder & Sommerfeld, 2007). This avoids errors connected to separate measurements like slightly shifted flow fields or different raw water quality and therefore small amounts of unknown contaminations.

In the present work, a thin DOF of about 1 cm was adjusted in the center of the column as it is shown in Figure 1 on the right side. Objects inside this region are captured with sharp edges, while with increasing distance to this region the edges of captured objects are more and more blurred. As shown by Ziegenhein et al. 2018b the vertical velocity in the z-direction is constant only in the center region, which means that velocity gradients in the depth are present closer to the wall. Hence, only bubbles in the center region and

therefore sharp bubbles should be used for the lift force evaluation since z-derivations are neglected in the calculation. Additionally, possible wall effects influencing the lift force measurement can be avoided when only sharp bubbles in the center are used.

For the bubble identification, an algorithm based on a sobel operator is used, which calculates the pixel grey value derivative along the edges of an object. A threshold is then used to include only bubbles with strong enough, and therefore sharp edges. This threshold is calibrated to a distance of ±1 cm from the sharpness center and therefore double the size of the DOF. This range was chosen to ensure that enough bubbles are evaluated, which are still in the center region and therefore not effected by the mentioned problems close to the column walls. Bubbles out of this region are excluded from further investigations. An example is depicted in Figure 2 on the left side; the sharp bubble in the lower right corner is located inside the sharpness region, while the blurred bubble in the top left corner has too weak grey value derivatives and is therefore outside of the center region. After validating the bubbles according to their sharpness degree, geometric properties as well as the bubble velocity are determined. Important geometric properties are the major and minor axis as a representation of the shape and the spherical equivalent diameter. The major axis is defined as the larges extend of the projected bubble and the minor axis as the largest extent perpendicular to the major axis (Ziegenhein & Lucas, 2017). For calculating the spherical equivalent diameter, the solid of revolution of the projected bubble is used. The bubble velocity is determined via tracking the centroid of the projected area of an identified bubble.

With the same sharpness principal, the liquid velocity is determined. The displacement of sharp tracer objects inside this sharpness region are used for calculating velocities from a pair of double images. This technique is designated as Particle Shadow Velocimetry (PSV) in the literature (Estevadeordal & Goss, 2005). Recently, Hessenkemper &

Ziegenhein 2018 introduced two processing procedures to determine the liquid velocity with this PSV technique, which are both used in the present work. The first procedure is called Particle Shadow Image Velocimetry (PSIV) and uses standard cross-correlation based methods to determine displacements of defined interrogation areas, as it is usually done in PIV processing tools. This procedure includes a bubble mask to exclude bubble shadows in the velocity interrogation and a so-called particle sharpening step. The latter can be used to manipulate the DOF via pronouncing sharp particles in comparison to blurred particles in the correlation step. The second procedure is called Particle Shadow Tracking Velocimetry (PSTV), which identifies sharp tracer particles based on their grey value derivative like for the single bubbles. These tracers are then tracked in an image pair to determine the liquid velocity.

To measure the liquid velocity with the PSIV method, the flow was seeded with 100 µm Polyamid Seeding Particles. An example image with determined displacement vectors is given in Figure 2 on the left side. As it can be seen, next to the tracer particles and the single bubbles also intermediate sized structures are present in the flow. These structures are not particle agglomerates but microbubbles in the size range of several hundred µm generated by the system itself. As it was demonstrated by Ziegenhein et al. 2016 or Truong et al. 2018 such microbubbles can be used as tracers when the size is small enough. Therefore, the liquid velocity could also be measured without adding tracer particles but tracking sharp microbubbles. The right side of Figure 2 shows microbubble velocities determined with the PSTV method when no particles were added to the flow. The use of both techniques also enables the investigation of possible contamination effects of the used tracer particles on the single bubbles since the tracers where hydrophobic and attached to the bubble surfaces.

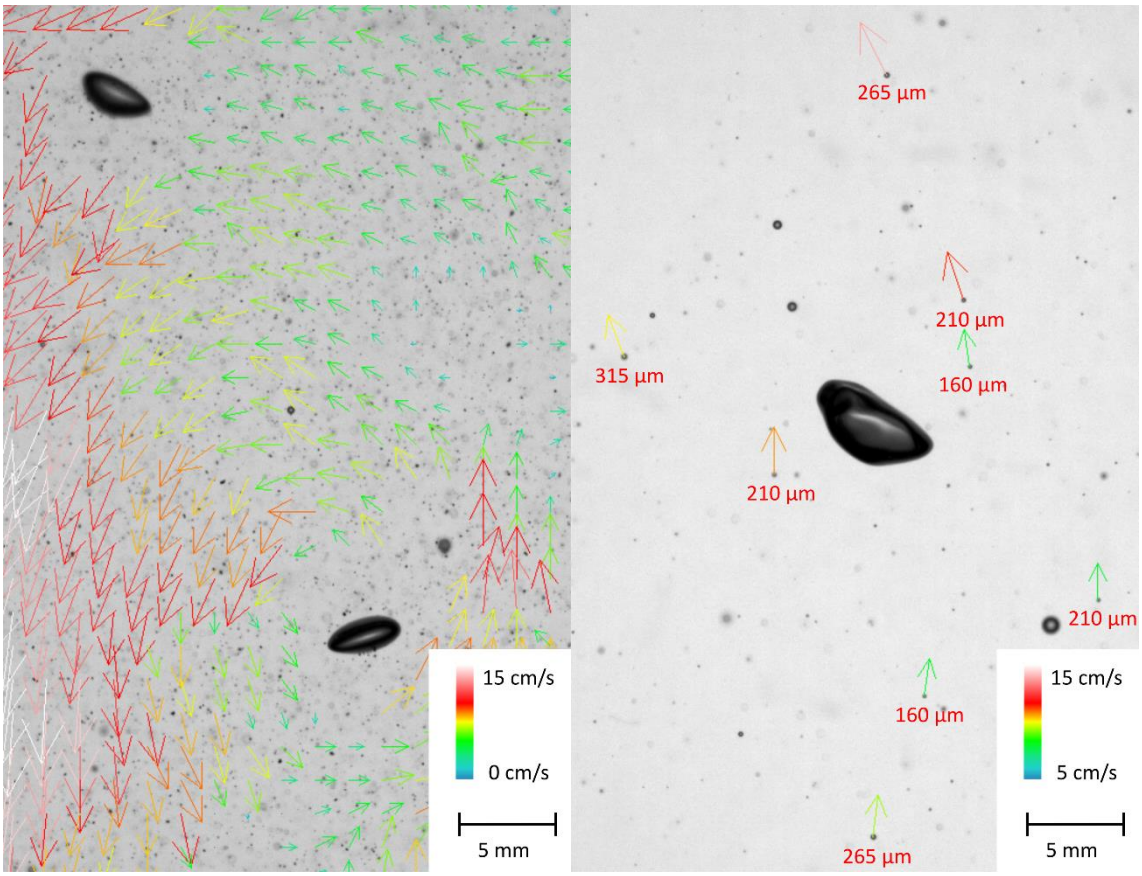

Figure 2: Cropped example images with liquid velocities. Left: PSIV velocity field with a sharp bubble and a blurred bubble outside the sharpness field ($Eo = 1.13$, 0.2 mol/l NaCl); Right: Tracked microbubbles and their sizes using the PSTV method around a wobbling bubble ($Eo = 3.57$, 1.0 mol/l NaCl).

For the present investigation, a distance of ± 5 mm from the center of the sharpness region was used for the particle sharpening as well as the microbubble identification, which corresponds to the thickness of the DOF. A difficulty that arises due to the added NaCl is that the amount of microbubbles increases with increasing NaCl concentration. This could cause problems when particles are added to the flow, since particles and microbubbles show different densities and a distinction between small sized microbubbles and the tracer particles is not possible in the images. Hence, the comparison with and without tracer particles was only conducted for the lowest investigated concentration of 0.2 mol/l NaCl, since the amount of microbubbles was low enough to not affect measurements with particles significantly, but still high enough to obtain average velocity fields with

reasonable statistic. For the higher concentrations, only the PSTV method with tracking microbubbles was used.

3. Results

3.1. Liquid vortex

The liquid vortex and its shear field are crucial for the lift force determination. Since the flow field is generated by bubbles itself, an increased bubble drag due to a NaCl contamination could change the shear field and therefore the governing shear rate too. Although Aoyama et al. 2017 as well as Ziegenhein et al. 2018b revealed no effect of the shear rate on C_L for non-spherical bubbles, an adoption of this observation is not possible when contaminations are present. The distribution of the absorbed salt molecules at the bubble surface might depend on the shear rate, which could lead to shear rate depended contamination effects. To examine the shear field generated by the driving bubbles, exemplary velocity profiles taken at the same height are shown in Figure 3 (a). Although the profiles show small differences, no systematic trend according to the NaCl concentration can be identified, which implies no strong salt effect on the driving bubbles and therefore on the liquid vortex for the investigated NaCl concentrations. A more likely explanation for these differences is a unique position of each generated vortex, meaning that the vortex core position slightly differs for different experiments. A possible reason for this could result from the filling process of each experiment. The water is filled through a funnel at the top of the column, while the gas bubbles are already generated at the bottom, so that the acceleration of the liquid through the driving bubbles starts already at the beginning of the filling process. Small deviations during this filling process could therefore cause hysteresis effects, which lead to slightly shifted vortex positions. However, this underlines the use of the sharpness technique and a simultaneous bubble and liquid velocity determination so that mismatching positions due to separated

measurements are avoided. Furthermore, the average shear field strength for different experiments is almost the same. Hence, the lift force is evaluated with an average shear rate of about 2.4 s^{-1} along the bubble path and possible shear rate dependent contamination effects are excluded.

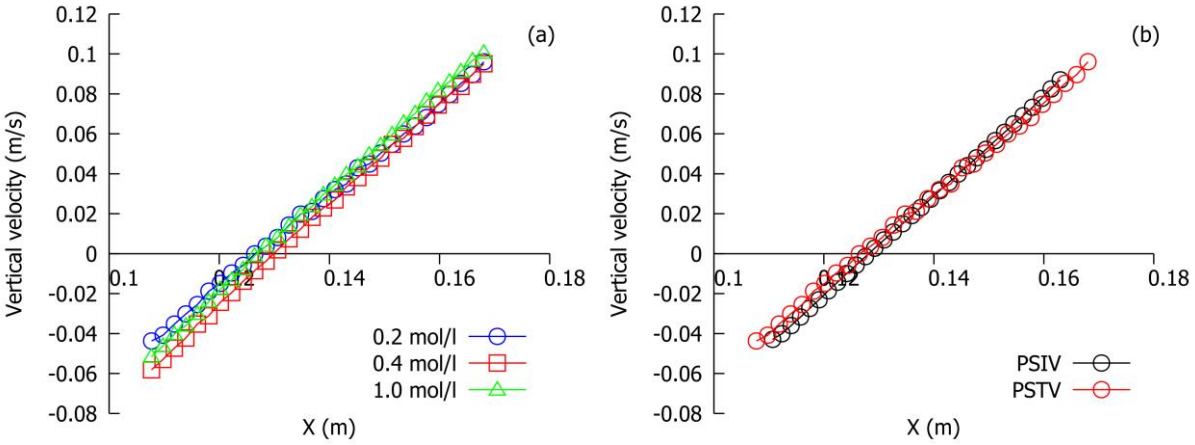

Figure 3: Liquid velocity profiles at the center of the vortex (Y=0.65 m). (a) Profiles for different NaCl concentrations obtained with the PSTV method, (b) Comparison of the used velocity determination methods with the same NaCl concentration of 0.2 mol/l.

A comparison of the used velocity determination techniques is shown in Figure 3 (b). The profile obtained with the PSIV method and added particles is a little bit smoother, which is caused by the larger number of velocities gathered with one image pair in comparison to tracking a lower number of microbubbles (cf. Figure 2). Nevertheless, the profiles are almost similar and no distinct difference could be observed. Since the liquid velocity is not affected by the presence of the tracer particles, it is possible to examine if the hydrophobic tracer particles have an impact on the gas phase, especially on the lift force.

3.2. Gas phase

The amount of absorbed NaCl molecules and therefore the contamination level of a bubble depends on its traveling time though the liquid (Kracht & Finch, 2010). Therefore, it should be noted that all following observations regarding contamination effects are only valid for the specific traveling time of about 2-3 s after the bubbles were generated at the sparger. Since the background flow can have an impact on the shape especially for smaller

bubbles (Ziegenhein & Lucas, 2017), the same applies for the bubble shape results with the specification of a liquid shear field in the background.

The investigated bubble sizes in this work are in the ellipsoidal bubble shape regime with a wobbling bubble surface according to the shape diagram of Grace et al. 1976 for clean bubbles. Due to this wobbling motion the captured shape from a bubble projection represents only a temporary state of the bubble surface. Hence, a large number of captured bubbles are required to calculate reliable average values and gather the full bandwidth of bubble surface states. Figure 4 shows several major axis size distributions of the lowest and the highest investigated NaCl concentrations for experiments with almost the same average spherical equivalent diameter as indicated in the figure legend. With increasing bubble size the distributions are spread, which means the wobbling effect gets stronger. Furthermore, the major axis of smaller bubbles is shifted to smaller values for similar bubble sizes indicating that the salt has an effect on the major axis and therefore on the bubble shape. However, the spherical equivalent diameters of these bubbles are also slightly different, so that the shift of the major axis might be caused by the different bubble size. The major axis of larger bubbles is not affected, whereby the spherical equivalent diameter is quite the same in that case. This implies that only for smaller bubbles the contamination is strong enough to reduce the bubble deformation.

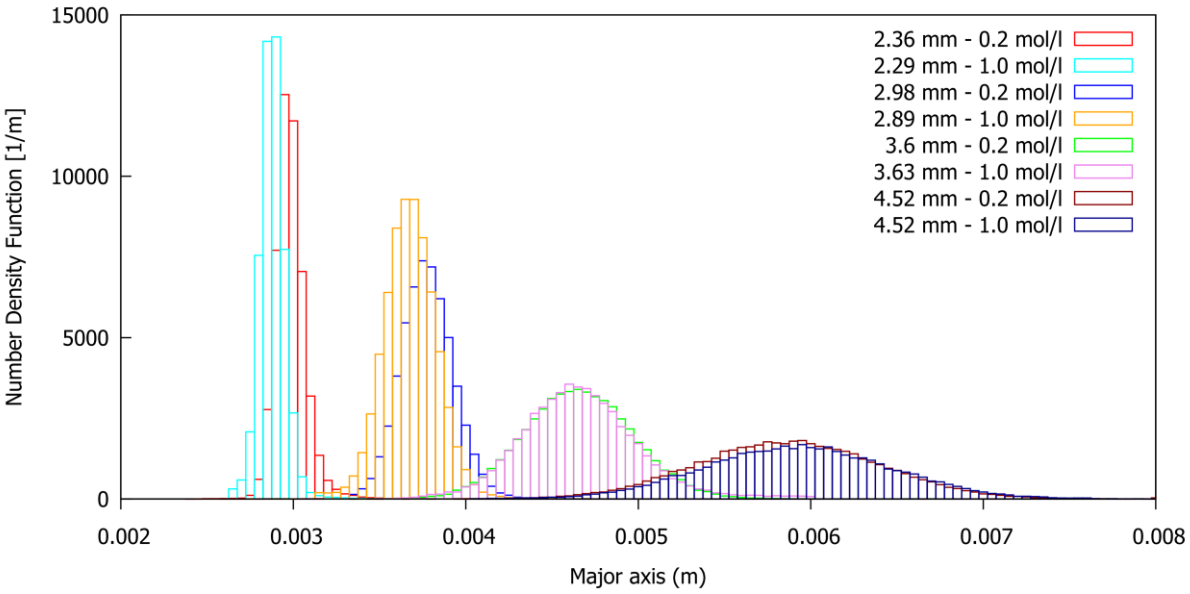

Figure 4: Major axis distribution of bubbles with the same diameter and different NaCl concentrations

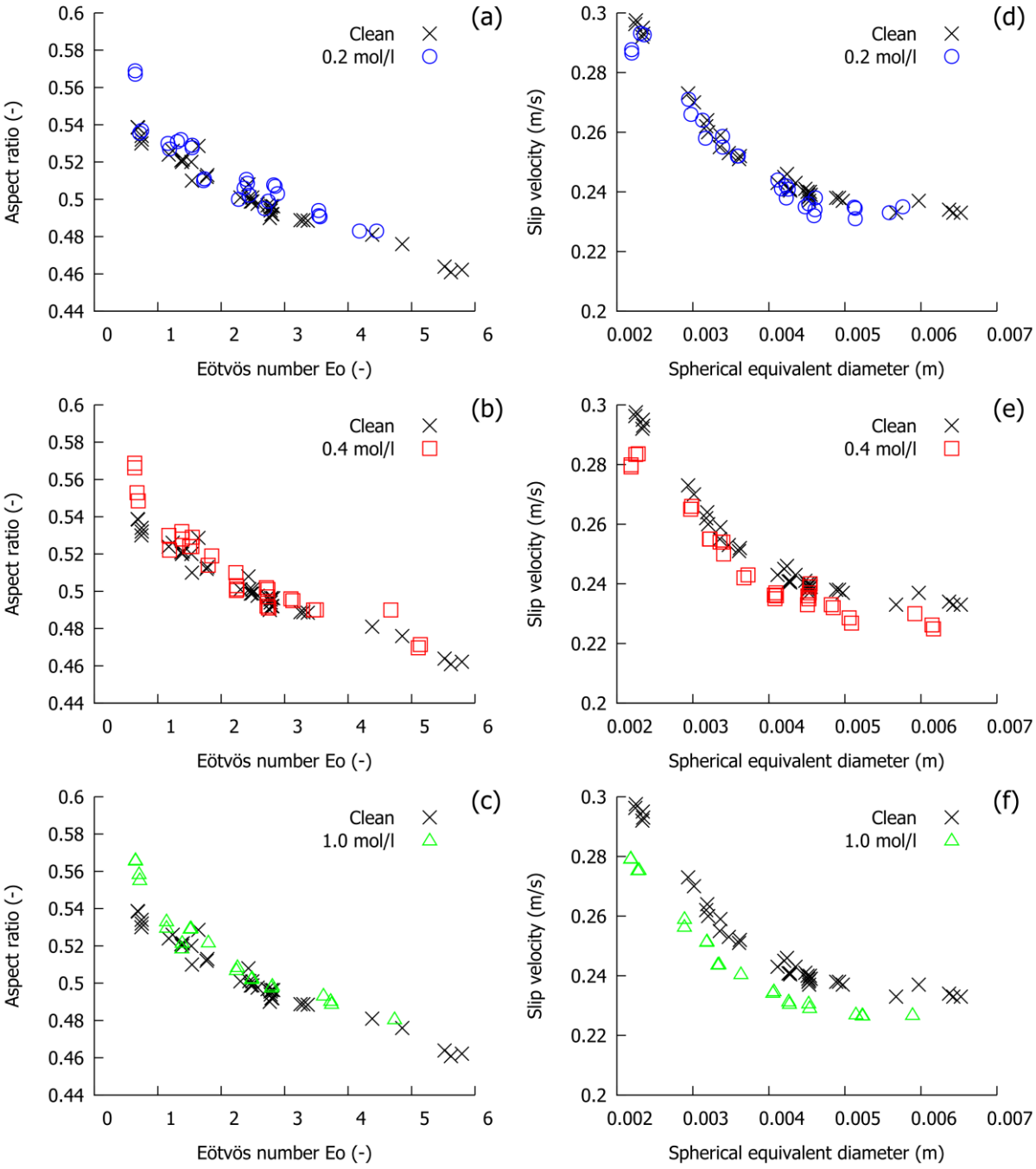

Figure 5: Comparison of shape (a-c) and slip velocity (d-f) in dependence of different NaCl concentrations to the 'Clean' reference from Hessenkemper et al. 2018

For a more specific analysis of ongoing bubble contaminations, the average results of every single experiment are compared with recent results from Hessenkemper et al. 2018 without the addition of contaminating substances, which are named “Clean” in the following. These clean results were obtained with the same measurement arrangement and settings, which means that also the PSV technique with simultaneous bubble and

liquid velocity determination was used. Therefore, it is more suitable to use these results for a comparison than the original results from Ziegenhein et al. 2018b.

As mentioned previously not only the shape but also the bubble slip velocity can be used as an indicator for present contaminants. Hence, both values are individually compared to the clean reference in Figure 5. The aspect ratio shows no significant change with respect to the clean data for all bubble sizes $Eo > 1$ (Figure 5 a-c). This means that the major axis changes observed for the bubbles $d_B \approx 2.9\,mm$ ($Eo \approx 1.1$) in Figure 4 are more related to the smaller bubble size than to a contamination effect. The smallest bubbles however show an increase of the aspect ratio for all NaCl concentration, while the aspect ratio of bubbles in the range $Eo = 0.68 - 0.75$ are increased in dependence of the salt concentration. Therefore, the major axis changes of the smallest bubbles $d_B \approx 2.3\,mm$ ($Eo \approx 0.7$) in Figure 4 are a result of a reduced deformation caused by the higher salt concentration. A more detailed analysis of these smaller bubbles follows in section 3.3.2.

The situation is a little bit different when the bubble slip velocity is used to evaluate ongoing contamination effects. For the lowest investigated concentration of 0.2 mol/l NaCl the results match the clean data quite well except for the smallest bubble size again (Figure 5 d). With increasing NaCl concentration the slip velocity of all bubbles is decreased in comparison to the clean case (Figure 5 e-f). This indicates that the contamination effect of NaCl on the shape is different to the effect on the slip velocity, which has also been reported in the literature (Maldonado, et al., 2013). Therefore, the following analysis of the lift coefficient behavior will address both values individually to clarify if a possible contamination effect on C_L is more connected to a change of the shape or a change of the slip velocity.

3.3. Lift coefficients

3.3.1. C_L results

All obtained lift coefficients are plotted against the modified Eötvös number $Eo_\perp$ in Figure 6, whereby the different concentrations are again compared separately to the clean reference case. Figure 7 shows the same results for all concentrations combined. As the bubble shape and slip velocity are the same for most of the bubbles of the clean case and the 0.2 mol/l salt concentration, also the lift coefficients are not changed as can be seen in Figure 6a. However, for the smallest bubbles two measuring points are affected by the presence of NaCl; for those two measuring points the bubble shape and slip velocity are also affected (cf. Figure 5 a and d). These two measurings show increased lift coefficients in comparison to the reference, while all larger bubble sizes match the clean data quite well. The same trend can be observed for a concentration of 0.4 mol/l NaCl, which is depicted in Figure 6b. Again, measurings with a clear change of the shape and the slip velocity show increased C_L values in comparison to clean bubbles, while no change is present for larger bubbles. For the highest concentration of 1.0 mol/l NaCl a change of the aspect ratio is still present only for the smallest bubbles (cf. Figure 5c), whereas higher C_L's can be observed also for larger bubbles (Figure 6c and Figure 7). However, these larger bubbles show clear changes of the slip velocity (cf. Figure 5f). In this case, a connection of C_L changes caused by contaminations might be more suitable with the use of the slip velocity.

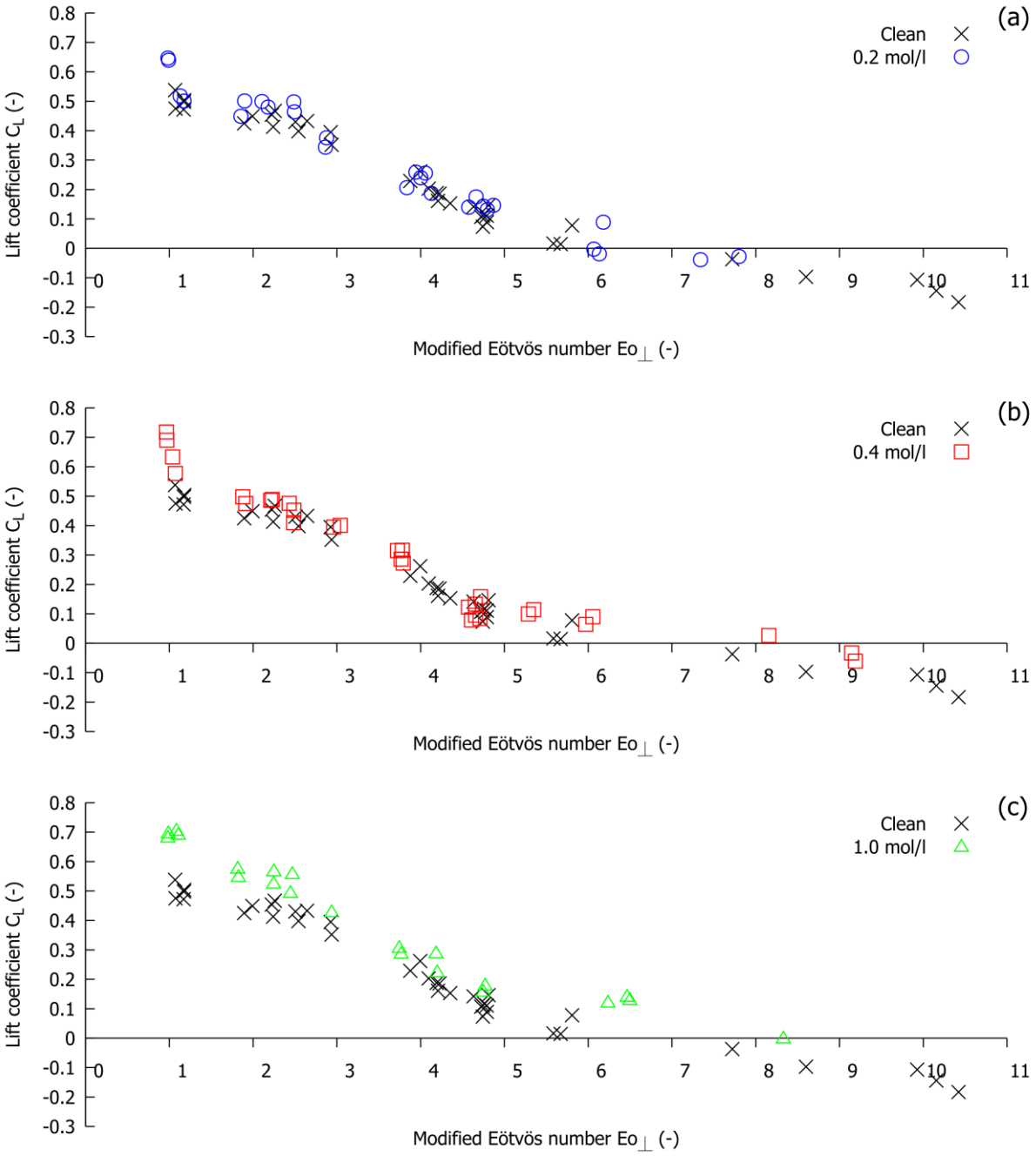

Figure 6: Results of the lift force measurements for (a) 0.2 mol/l (b) 0.4 mol/l and (c) 1.0 mol/l NaCl in comparison to the 'Clean' reference from Hessenkemper et al. 2018

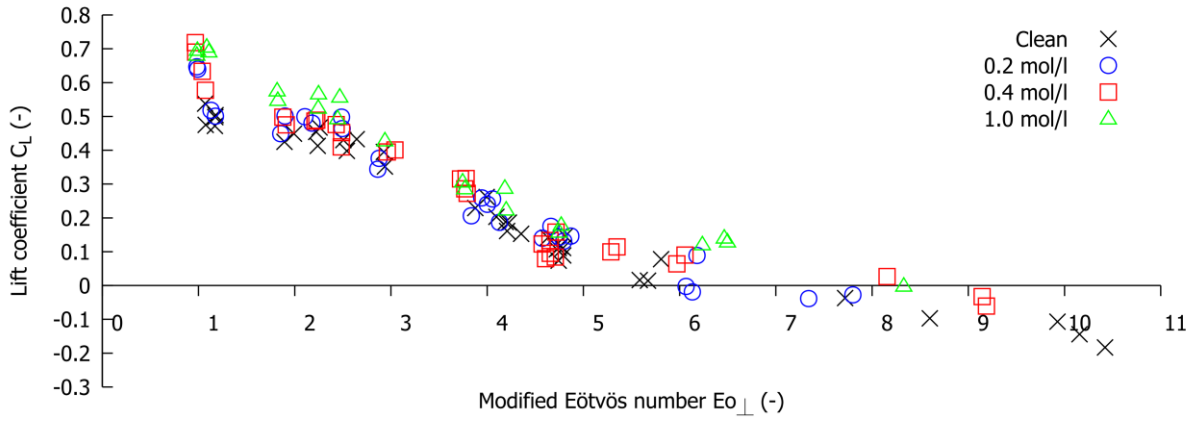

Figure 7: Lift coefficients in dependence of the modified Eötvös number

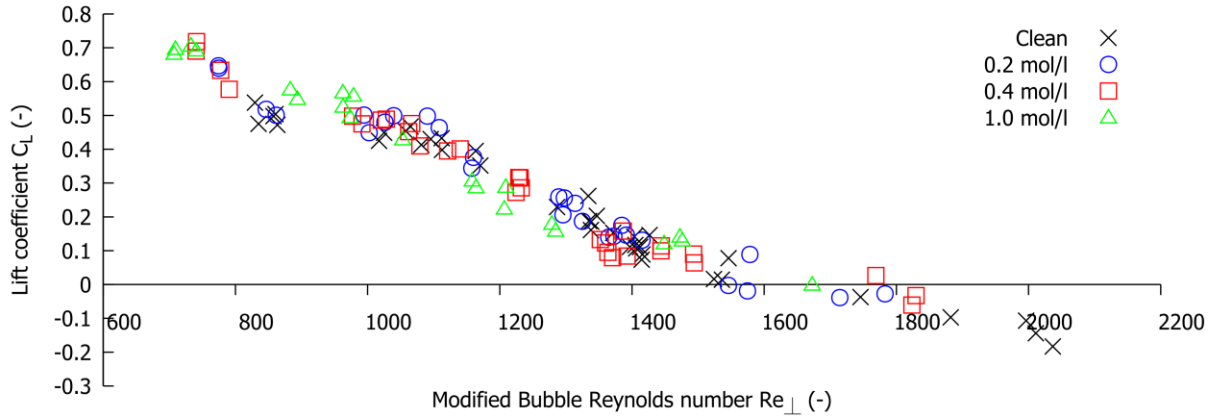

Figure 8: Lift coefficients in dependence of the modified bubble Reynolds number

The results demonstrate, that the behavior of C_L in saline solutions can not be described with changes of the bubble shape only. The modified Eötvös number $Eo_\perp$ fails to capture all differences caused by contaminations, since it only addresses differences connected to the major axis, while velocity-based changes are left aside. Nevertheless, strong increases of C_L are also reflected in a reduced bubble deformation. For this reason, the modified Reynolds number $Re_\perp$ might be more suitable to describe the C_L behavior, since it includes changes of the slip velocity as well as changes of the shape. Figure 8 shows all lift force results in dependence of the modified Reynolds number $Re_\perp$. The combined data match quite well for almost all bubble sizes and show a linear decrease of C_L over $Re_\perp$. Small clean bubbles however, do not completely fit into this trend, since in the clean case no

significant higher C_L values than 0.5 could be observed. This value has also been reported for spherical bubbles with high Reynolds numbers in the literature (Auton, 1987) (Legendre & Magnaudet, 1998), so that 0.5 might be a limitation for smaller clean bubbles. According to the present results it seems that this limitation is increased to at least 0.7 by the presence of NaCl. However, the smallest bubbles investigated in this work are still ellipsoidal and not spherical, so that further data with smaller bubbles is required to prove this statement.

3.3.2. Contamination on small bubbles

Since the previous results show that the most significant changes occur for smaller bubbles, a detailed analysis of bubbles $Eo < 1$ was done. Figure 9 shows the results for the bubble shape and the slip velocity for the two smallest investigated bubble sizes, while Figure 10 shows the corresponding lift coefficients. The smallest bubbles in this work ($Eo = 0.64$) have the same aspect ratio of about 0.57 independent of the NaCl concentration (Figure 9a). I contrast, the smallest bubbles of the clean reference ($Eo = 0.68$) show a slightly stronger deformation with an aspect ratio of about 0.54. Since the deformation does not change with increasing salt concentration, bubbles of this size might be already in an equilibrium contamination state, which means that higher concentrations or longer traveling times would not affect the aspect ratio anymore. However, only the two highest concentrations show the same slip velocity for this bubble size, while the values of the 0.2 mol/l concentration are situated between the clean case and the two others (Figure 9b). Therefore, the smallest bubbles of the concentrations 0.4 mol/l and 1.0 mol/l are most likely in an equilibrium contamination state, while for the concentration of 0.2 mol/l these bubbles are still less contaminated. These observations also follow the description of a different shape-velocity behavior with respect to the contamination level.

The lift coefficients of these smaller bubbles (Figure 10) follow the trend of the slip velocity; the equal contaminated bubbles show a C_L of about 0.7, while the partially contaminated bubbles of the lowest NaCl concentration show a slightly reduced C_L of about 0.65. This underlines the statement, that the slip velocity might be a better contamination indicator in saline solutions with respect to changes of C_L.

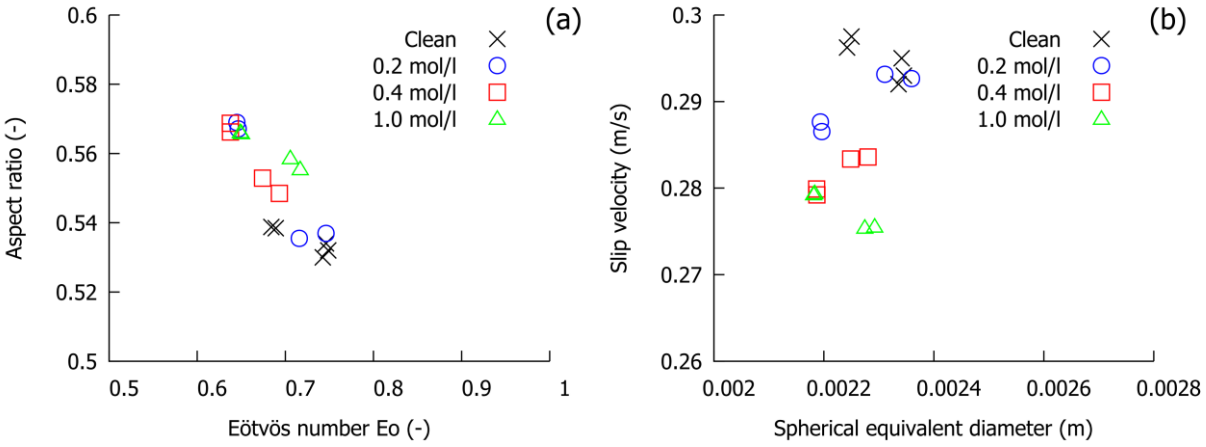

Figure 9: Detailed analysis of NaCl concentration dependent contamination effects on (a) shape and (b) slip velocity for small bubbles (Eo<1)

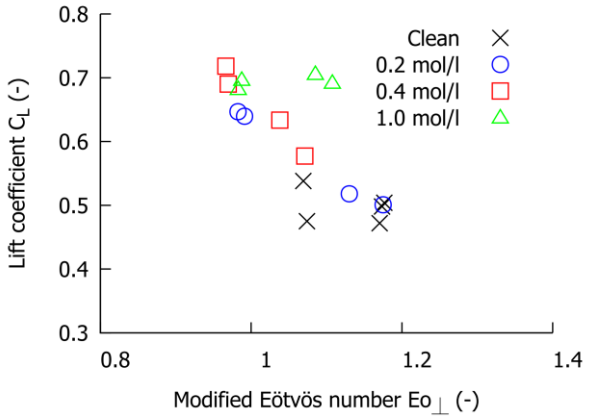

Figure 10: Lift force results for small bubbles

The next larger bubbles show a stronger correlation of the bubble shape and velocity in dependence of the governing NaCl concentration. For the lowest concentration of 0.2 mol/l no distinct increase of the aspect ratio as well as a decrease of the slip velocity can be observed in comparison to the clean data, which is also reflected in an unaffected C_L

for this bubble size. However, the aspect ratio is increased, and the slip velocity is decreased for the two higher NaCl concentrations. The C_L values follow the same trend again as the smallest bubbles; the less contaminated bubbles with respect to the shape and slip velocity show slightly increased C_L values, while the stronger contaminated bubbles show a stronger increase of C_L.

3.3.3. Influence of hydrophobic particles

As stated before, the concentration of 0.2 mol/l NaCl enables the investigation of possible effects of hydrophobic tracer particles on the single bubbles. Again, the focus is on the three bubble properties that are connected to contamination influences in this work, namely the shape, slip velocity and the lift coefficient. These values are depicted in Figure 11 and Figure 12, whereby the results are separated according to the liquid velocity determination technique. Consequently, the results for the PSIV method are obtained with added tracer particles and the results for the PSTV method are obtained with microbubbles and therefore without particles. Obviously, no systematic change in the shape can be identified (cf. Figure 11a). The slip velocity is also quite the same, although slightly higher values are derived for bubbles in the size range $d_B = 3 - 3.5\,mm$ with added particles. However, an increase of the slip velocity due to the attached particles is not plausible. Although it has been proven in Figure 3b that the results obtained with the PSIV/particle method and the PSTV/microbubble method are almost the same, the amount of gained liquid velocities with the latter is significantly smaller, which might result in a not sufficient statistic and therefore a less accurate average value. Therefore, no clear contamination effect with respect to the bubble shape and slip velocity could be identified by the presence of hydrophobic tracer particles.

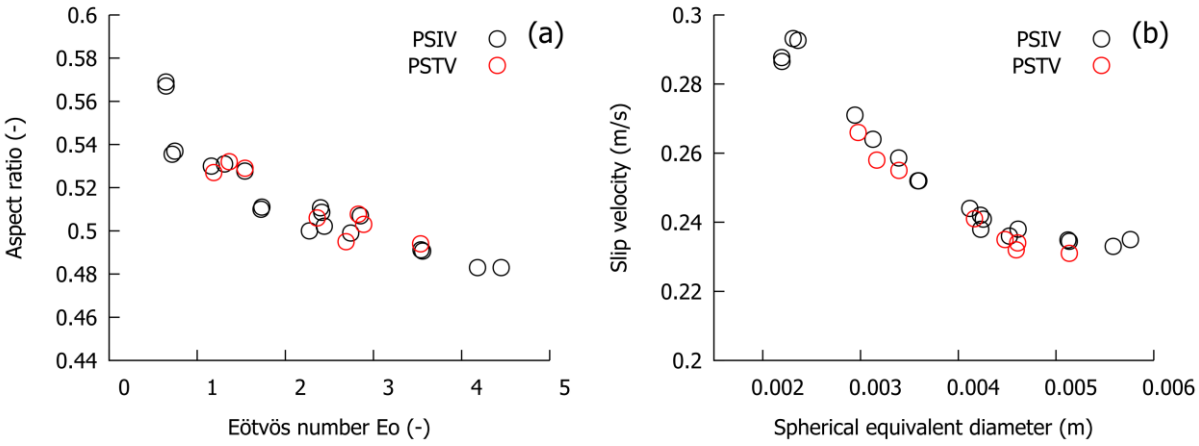

Figure 11: Influence of measurements with (PSIV) and without (PSTV) added particles on the bubble (a) shape and (b) slip velocity

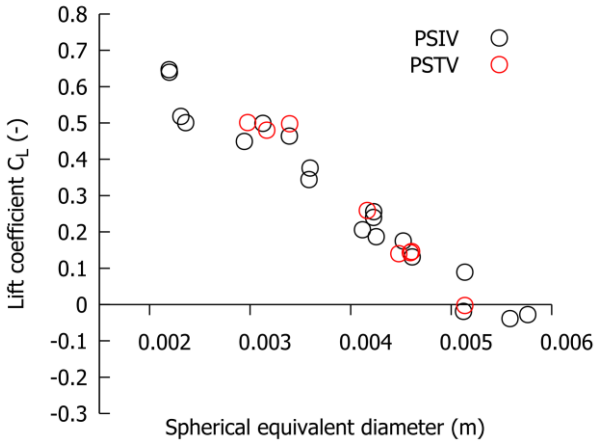

Figure 12: Lift force results with (PSIV) and without (PSTV) added particles

Although these minor differences of the slip velocity are present for smaller bubbles, no effect of the method or the presence of particles can be identified with respect to C_L (cf. Figure 12). Thus, it is possible to determine and compare lift coefficients obtained with both methods and with or without particles. This is important regarding the comparability to the clean reference case, since the results of the clean case were gathered with the PSIV/particle method, while most results of this work were gained with the PSTV/microbubble method. Obviously, a rather small seeding concentration was chosen to not affect the measurement, which is confirmed hereby. Nevertheless, the findings according to hydrophobic particle effects are again only valid for the previously

mentioned bubble travel time and background liquid flow for the same reasons, as well as the limitation of small particle concentrations.

4. Conclusion and discussion

The influence of different NaCl contamination levels on the lateral lift force of single bubbles rising through a linear shear field has been investigated in the present work. For this, a recently developed method by Ziegenhein et al. 2018b was used, which is capable to overcome common difficulties of low viscous systems like producing a strong enough shear field or handling irregular bubble movements. With that, ellipsoidal bubbles in the size range of 2.2 – 6.5 mm spherical equivalent diameter were investigated and compared to a clean reference case, which was obtained with the same measurement arrangement and settings (Hessenkemper, et al., 2018). Special attention was drawn on the bubble shape and slip velocity, as both values are indicators of ongoing contamination processes at the bubble surface.

The use of a small DOF enabled simultaneous measurements of necessary bubble properties and liquid velocities. For the latter, the Particle Shadow Velocimetry (PSV) method was used, with which the liquid velocity could be determined with two different procedures. The Particle Shadow Image Velocimetry (PSIV) procedure uses slightly adapted PIV processing techniques and requires the addition of tracer particles, while the Particle Shadow Tracking Velocimetry (PSTV) procedure is able to determine the liquid velocity via tracking natural occurring microbubbles, so that no tracer particles had to be added. Furthermore, the small DOF allowed to distinguish between sharp bubbles in the column center and blurred bubbles outside of the sharpness region. Therefore, only sharp bubbles were evaluated to exclude unknown wall effects or velocity gradients in the depth, which could bias the lift force evaluation.

Three different NaCl concentration were investigated, namely 0.2 mol/l, 0.4 mol/l and 1.0 mol/l. A clear contamination effect in terms of a reduced oblateness and slip velocity could be designated only for the smallest investigated bubbles of about 2.2 mm diameter. With increasing NaCl concentration slightly larger bubbles showed also a reduced deformation, whereby the contamination level clearly depends on the bubble size and the governing concentration. According to investigations of the bubble shape with added NaCl in the literature, the present results are more relatable to the results obtained by Ziegenhein et al. 2018a than the results by Quinn et al. 2014. Nevertheless, significant deformation changes of small bubbles were not found in the former source. Here the specification of the bubble traveling time or the background flow might be the reason for the different findings. The slip velocity showed a slightly different behavior. For lower concentrations, only bubbles with a clear reduced deformation showed also decreased velocities. With increasing salt concentration however, also larger bubbles showed decreased slip velocities, although no change of the shape could be observed.

The previously mentioned smallest bubbles with clear shape and velocity changes showed also a significant increase of the lift coefficient in comparison to the clean case. For larger bubbles, only small increases of C_L could be observed with the highest NaCl concentration of 1.0 mol/l. Since these bubbles did not show a change of the shape but slightly reduced velocities, the slip velocity is more suitable as an indicator of contamination effects which can be directly connected to changes of C_L. Since the shape does not reflect all C_L changes, the modified Eötvös number $Eo_\perp$ might be not the first choice to address the lift coefficient changes for different NaCl concentrations in a saline air-water system. The modified Reynolds number $Re_\perp$, as it is based on the slip velocity and the major axis as the characteristic length scale, appeared to be more appropriate, since strong C_L increases still go along with a reduced major axis, while small changes are

only connected to the slip velocity. However, it appears that the effect is different to that caused by organic surfactants, since lift coefficients are decreased according to the literature when such kind of substances are present in the liquid phase. This might imply that the changes of C_L caused by contaminations are dependent on the direction of the surface tension gradient and therefore the acting direction of the Marangoni-stress, since most inorganic surfactants like NaCl increase, while organic surfactants decrease the surface tension.

As reported by Lucas et al. 2005, positive C_L values stabilize the flow and counteract the establishment of maxima in the velocity profile in buoyancy driven flows. Such maxima can lead to a regime transition in bubbly flows (Lucas, et al., 2005). These positive C_L values are mostly observed for small bubbles in the literature, which is also the case in the present investigation. A shift of the critical bubble size for the C_L sign change caused by additives could therefore result in a shift of the regime transition. This could pronounce the development of a homogenous flow regime if the critical size is increased. Regarding this critical size, no distinct change can be observed for concentrations up to 0.4 mol/l. This means that up to this concentration shifts of the regime transition reported in the literature (Besagni & Inzoli, 2017) are more likely connected to the prevention of bubble coalescence and a shift of the bubble size distribution to smaller bubbles, than a change of the critical size of the C_L sign change. For higher salt concentrations however, a shift of the critical equivalent diameter from about 5.1 mm for clean bubbles to around 6 mm for a concentration of 1.0 mol/l could be observed. This could contribute to a shift of the regime transition, although the former mentioned coalescence inhibition and smaller bubble sizes might still be the main reasons for this.

As described, the addition of NaCl influences the bubbles in several ways. Beside the changed single bubble behavior, the amount of generated microbubbles increased with

increasing NaCl concentration, which had the consequence that only the PSTV/microbubble method was applicable to determine the liquid velocity for the two higher used concentrations. For the NaCl concentration of 0.2 mol/l both methods were applicable, which allowed a comparison of measurements with added tracer particles and without. Since the used tracer particles were hydrophobic, some of them attached to the bubble surface and could therefore also influence the bubble behavior. Nevertheless, the results revealed no change in either the shape nor the slip velocity, as well as a similar C_L in comparison to the PSTV method without the addition of tracer particles.

Overall, a clear influence of NaCl contaminations on the lateral lift force could be identified in the present work, whereby these changes are more reflected in contamination caused changes of the slip velocity than changes of the bubble shape. Since NaCl is a rather weak surfactant, these changes are however mostly relevant for higher concentrations or smaller bubbles. This could be quite different for strong organic surfactants, which has been shown to influence the lift force significantly at least for smaller bubbles in the past (Takagi & Matsumoto, 2011). Further measurements regarding this topic are planned and should help to clarify how impurities influence the flow behavior of bubbly flows. Nevertheless, the present results might be helpful to design further CFD-grade experiments, since the use of small salt concentrations enables the inhibition of coalescence, while other parameters like the bubble drag or the lift force are not affected, at least for bubbles $Eo > 1$.

References

Adoua, R., Legendre, D. & Magnaudet, J., 2009. Reversal of the lift force on an oblate bubble in a weakly viscous linear shear flow. *J. Fluid Mech.,* Volume 628, pp. 23-41.

Aoyama, S. et al., 2017. Lift force acting on single bubbles in linear shear flows. *Int. J. Multiphase Flow,* Volume 96, pp. 113-122.

Aoyama, S., Hayashi, K., Hosokawa, S. & Tomiyama, A., 2018. Shapes of single bubbles in infinite stagnant liquids contaminated with surfactant. *Exp. Therm. Fluid Sci.,* Volume 96, pp. 460-469.

Auton, T. R., 1987. The lift force on a spherical body in a rotational flow. *J. Fluid Mech.,* Volume 183, pp. 199-218.

Besagni, G. & Inzoli, F., 2017. The effect of electrolyte concentration on counter-current gas-liquid bubble column fluid dynamics: Gas holdup, flow regime transition and bubble size distributions. *Chem. Eng. Res. Des.,* Volume 118, pp. 170-193.

Bothe, D., Schmidtke, M. & Warnecke, H.-J., 2006. VOF-Simulation of the Lift Force for Single Bubbles in a Simple Shear Flow. *Chem. Eng. Technol.,* Volume 29, pp. 1048-1053.

Bröder, D. & Sommerfeld, M., 2007. Planar shadow image velocimetry for the analysis of the hydrodynamics in bubbly flows. *Meas. Sci. Technol.,* Volume 18, pp. 2513-2528.

Clift, R., Grace, J. & Weber, M., 1978. *Bubbles, Drops and Particles.* New York: Academic Press.

Cuenot, B., Magnaudet, J. & Spennato, B., 1997. The effects of slightly soluble surfactants on the flow around a spherical bubble. *J. Fluid Mech.,* Volume 339, pp. 25-53.

Dijkhuizen, W., van Sint Annaland, M. & Kuipers, J., 2010. Numerical and experimental investigation of the lift force on single bubbles. *Chem. Eng. Sci.,* Volume 65, pp. 1274-1287.

Ervin, E. & Tryggvason, G., 1997. The Rise of Bubbles in a Vertical Shear Flow. *J. Fluids Eng.,* Volume 119, pp. 443-449.

Estevadeordal, J. & Goss, L., 2005. *PIV with LED: Particle Shadow Velocimetry (PSV).* Reno, Nevada, 43rd AIAA Aerospace Sciences Meeting and Exhibit.

Fan, L.-S. & Tsuchiya, K., 1990. *Bubbly wake dynamics in liquids and liquid-solid suspensions.* s.l.:Butterworth-Heinemann.

Firouzi, M., Howes, T. & Nguyen, A., 2015. A quantitative review of the transition salt concentration for inhibiting bubble coalescence. *Adv. Colloid and Interface Sci.,* Volume 222, pp. 305-318.

Fukuta, M., Takagi, S. & Matsumoto, Y., 2008. Numerical study on the shear-induced lift force acting on a spherical bubble in aqueous surfactant solutions. *Phys. Fluids,* Volume 20.

Grace, J. R., Wairegi, T. & Nguyen, T. H., 1976. Shapes and velocities of single drops and bubbles moving freely through immiscible liquids. *Transact. Inst. Chem. Eng. ,* Volume 54, pp. 167-173.

Hayashi, K. & Tomiyama, A., 2018. Effects of surfactant on lift coefficients of bubbles in linear shear flows. *Int. J. Multiphase Flow,* Volume 99, pp. 86-93.

Hessenkemper, H. & Ziegenhein, T., 2018. Particle Shadow Velocimetry (PSV) in bubbly flows. *Int. J. Multiphase Flow,* Volume 106, pp. 268-279.

Hessenkemper, H., Ziegenhein, T. & Lucas, D., 2018. Lift force measurements of ellipsoidal single bubbles in water. *Phys. Fluids, submitted.*

Hosokawa, S., Masukura, Y., Hayashi, K. & Tomiyama, A., 2017. Experimental evaluation of Marangoni stress and surfactant concentration at interface of contaminated single spherical drop using spatiotemporal filter velocimetry. *Int. J. Multiphase Flow,* Volume 97, pp. 157-167.

Kariyasaki, A., 1987. *Behavior of a single gas bubble in a liquid flow with a linear velocity profile.* Honolulu, Hawaii, ASME/JSME Thermal Engineering Joint Conference.

Kracht, W. & Finch, J. A., 2010. Effect of frother on initial bubble shape and velocity. *Int. J. Min. Proc.,* Volume 94, pp. 115-120.

Krzan, M., Lunkenheimer, K. & Malysa, K., 2004. On the influence of the surfactant's polar group on the local and terminal velocities of bubbles. *Coll. Surf. A,* Volume 250, pp. 431-441.

Legendre, D. & Magnaudet, J., 1997. A not on the lift force on a spherical bubble or drop in a low-Reynolds-number shear flow. *Phys. Fluids,* Volume 9, pp. 3572-3574.

Legendre, D. & Magnaudet, J., 1998. The lift force on a spherical bubble in a viscous linear shear flow. *J. Fluid Mech.,* Volume 368, pp. 81-126.

Liu, Y.-S.et al., 2009. Viscosity and Density of the System NaCl + LaCl3 + H2O and Its Binary Subsystems at Different Temperatures. *J. Chem. Eng. Data,* Volume 54, pp. 739-744.

Lucas, D., Prasser, H.-M. & Manera, A., 2005. Influence of the lift force in the stability of a bubble column. *Chem. Eng. Sci.,* Volume 60, pp. 3609-3619.

Lucas, D. & Tomiyama, A., 2011. On the role of the lateral lift force in poly-dispersed bubbly flows. *Int. J. Multiphase Flow,* Volume 37, pp. 1178-1190.

Lu, J., Muradoglu, M. & Tryggvason, G., 2017. Effect of insoluble surfactant on turbulent bubbly flows in vertical channels. *Int. J. Multiphase Flow,* Volume 95, pp. 135-143.

Maldonado, M., Quinn, J. J., Gomez, C. O. & Finch, J. A., 2013. An experimental study examining the relationship between bubble shape and rise velocity. *Chem. Eng. Sci.,* Volume 98, pp. 7-11.

Nayar, K., Panchanathan, D., Mckinley, G. & Lienhard, J., 2015. Surface Tension of Seawater. *J. Phys. Chem. Ref. Data,* Volume 43.

Orvalho, S., Ruzicka, M. & Drahos, J., 2009. Bubble Column with Electrolytes: Gas Holdup and Flow Regimes. *Ind. Eng. Chem. Res.,* Volume 48, pp. 8237-8243.

Quinn, J., Maldonado, M., Gomez, C. & Finch, J., 2014. Experimental study on the shape-velocity relationship of an ellipsoidal bubble in inorganic salt solutions. *Minerals Engineering,* Volume 55, pp. 5-10.

Takagi, S. & Matsumoto, Y., 2011. Surfactant Effects on Bubble Motion and Bubbly Flows. *Annu. Rev. Fluid Mech.,* Volume 43, pp. 615-636.

Takagi, S., Ogasawara, T., Fukuta, M. & Matsumoto, Y., 2009. Surfactant effect on the bubble motions and bubbly flow structures in a vertical channel. *Fluid Dyn. Res.,* Volume 41, pp. 1-17.

Takagi, S., Ogasawara, T. & Matsumoto, Y., 2008. The effects of surfactant on the multiscale structure of bubbly flows. *Philos. Trans. R. Soc. A,* Volume 366, pp. 2117-2129.

Tomiyama, A., 2004. Drag, lift and virtual mass forces acting on a single bubble. 3rd International Symposium on Two-Phase Flow Modelling and Experimentation.

Tomiyama, A., Celata, G., Hosokawa, S. & Yoshida, S., 2002a. Terminal velocity of single bubbles in surface tension force dominant regime. *Int. J. Multiphase Flow,* Volume 28, pp. 1497-1519.

Tomiyama, A. et al., 1995. *Effects of Eötvös Number and Dimensionless Liquid Volumetric Flux on Lateral Motion of a Bubble in a Laminar Duct Flow.* Kyoto, Japan, Proceedings of the Second International Conference on Multiphase Flow.

Tomiyama, A., Tamai, H., Zun, I. & Hosokawa, S., 2002b. Transverse migration of single bubbles in simple shear flows. *Chem. Eng. Sci.,* Volume 57, pp. 1849-1858.

Troung, C. et al., 2018. Multiplane particle shadow velocimetry to quantify integral length scales. *Experiments in Fluids,* 59(4).

Ziegenhein, T., Garcon, M. & Lucas, D., 2016. Particle tracking using micro bubbles in bubbly flows. *Chem. Eng. Sci.,* Volume 153, pp. 155-164.

Ziegenhein, T. & Lucas, D., 2017. Observations on bubble shapes in bubble columns under different flow conditions. *Exp. Therm. Fluid Sci.,* Volume 85, pp. 248-256.

Ziegenhein, T., Lucas, D., Besagni, G. & Inzoli, F., 2018a. The Bubble Shape in Contaminated Bubbly Flows: Results for Different NaCl Concentrations in Purified Water. *ChemEngineering,* Volume 2.

Ziegenhein, T., Tomiyama, A. & Lucas, D., 2018b. A new measuring concept to determine the lift force for distorted bubbles in low Morton number system: Results for air/water. *Int. J. Multiphase Flow,* Volume 108, pp. 11-24.

Žun, I., 1980. The transverse migration of bubbles influenced by walls in vertical bubbly flow. *Int. J. Multiphase Flow,* Volume 6, pp. 583-588.